JMEPEG (2008) 17:920–927
DOI: 10.1007/s11665-008-9239-z

1059-9495/$19.00

Laser-Pulsed Heating of Aluminum: Cavity Formation at the Surface

B.S. Yilbas and S.B. Mansoor

(Submitted August 3, 2007; in revised form February 17, 2008)

Laser evaporative heating of aluminum surface is modeled numerically and mushy zone formation across the solid-liquid and the liquid-vapor phases is introduced in the model study. Temperature rise in the irradiated region and the cavity formation during the laser heating pulse are predicted. Temperature-dependent properties are introduced during the simulations. Oxygen diffusion into the substrate material is considered during the laser heating process while employing temperature-dependent diffusion coefficient. An experiment resembling the simulation conditions is carried out and the morphology of the cavity produced at the surface of the laser-irradiated region is examined using scanning electron microscopy (SEM) and atomic force microscopy (AFM). It is found that the depth of liquid phase increases significantly with the progressing time and the size of the mushy zone across the solid-liquid phase is smaller than that of across the liquid and the vapor phases. The cavity depth, observed from the SEM and AFM micrographs, is shallow and similar to those predicted from the numerical simulations.

Keywords aluminum, cavity, evaporation, heating, laser

1. Introduction

Lasers are widely used to modify the surface structure of metallic materials in relation to improved surface properties. Aluminum alloys are widely used in industry due to their low density; however, low tribological properties of the surface limits the wide usage of the alloys. Laser surface treatment technique is one of the methods, which improves the surface properties of the alloy with the low cost and the high precision. During the laser processing, oxide formation in the treated region is unavoidable despite the fact that aluminum alloys have low oxygen diffusion coefficients and shielding gas being used in the process. Although oxide layer is significantly thin, in some cases, it results in the surface cracks onset of the rapid solidification due to the non-uniform cooling rates of oxide components formed in the surface vicinity and the alloy constituents. However, the model studies provide insight into the physical processes taking place during the laser processing of the alloy. When modeling the laser heating situation, the phase change and oxidation in the laser-irradiated region should be considered in the analysis. In addition, the model study provides information, which will be useful to assess the evaporation depth and the resulting surface recession. Consequently, investigation into the laser heating of aluminum and oxidation at the surface becomes necessary.

Considerable research studies were carried out to examine the laser heating of aluminum surfaces. Excimer laser

B.S. Yilbas and **S.B. Mansoor**, Mechanical Engineering Department, KFUPM, Box 1913, Dhahran 31261, Saudi Arabia. Contact e-mail: bsyilbas@kfupm.edu.sa.

Nomenclature

Variables

a	Gaussian parameter (m)
A	Area (m^2)
Cp	Specific heat capacity (J/kg/K)
C	Concentration (wt.%)
C_o	Concentration at the surface (wt.%)
D	Diffusion coefficient (m^2/s)
h	Convective heat transfer coefficient ($W/m^2/K$); Sensible enthalpy (J/kg)
I_o	Laser power intensity (W/m^2)
k	Thermal conductivity (W/m/K)
L	Latent heat (J/kg)
m	Mass (kg)
r	Distance along the radial direction (m)
r_f	Reflectance
S	Source term (W/m^3)
T	Temperature (K)
T_o	Initial temperature (K)
t	Time (s)
x	Quality
z	Distance along the axial direction (m)

Greek symbols

δ	Reciprocal of absorption depth (m^{-1})
ρ	Density (kg/m^3)

Subscripts

b	vapor-liquid mushy zone; boiling
l	liquid
m	solid-liquid mushy zone; melting
o	initial value
ref	reference
s	solid, surface
v	vapor

interactions with an aluminum alloy were investigated by Koutsomichalis and Kefalidou (Ref 1). They indicated that the laser treatment resulted in the oxide and nitride formations at the surface through which surface properties were improved. The laser treatment of aluminum surface and corrosion resistance of the resulting surface was examined by Yue et al. (Ref 2). They showed that the grain boundaries of the re-solidified structure were free from precipitates and corrosion resistance of the surface improved significantly after the laser treatment process. A review on the laser treatment of aluminum alloys and corrosion properties was carried out by Watkins et al. (Ref 3). They indicated that the laser-treated alloy surface had unique microstructural and compositional characteristics, which improved hardness and the critical corrosion pitting potential. The residual stress produced in aluminum alloys by laser shock processing was investigated by Gomez-Rosas et al. (Ref 4). They showed that the surface residual stress level was higher with greater depths than that achieved by conventional shot peening process. The local surface modification of aluminum alloy by the laser irradiation was studied by Kikuchi et al. (Ref 5). They indicated that the key technology in the process is to use aluminum as a target for the laser irradiation in chemical solution and the anodic oxide film formed at the surface played an important role in the processes. The laser-induced aluminum surfaces and the plasma formation in the laser-irradiated region were investigated by Mazhukin et al. (Ref 6). They indicated that the vapor plasma pattern was characterized by the dense hot zone near the surface where the absorption of the laser energy took place, and the rapid decrease of density outside the zone occurred due to the plasma expansion. The mechanical and thermal effects induced by femtosecond laser treatment of aluminum single-crystal substrate were examined by Valette et al. (Ref 7). They showed that the crystallographic structure of the laser-produced surface was purer than the as-received surface and the laser effect was persistent on a typical scale of 10 μm below the surface. The laser melting of aluminum alloys and the corrosion protection were investigated by Davenport et al. (Ref 8). They indicated that the laser surface melting with an excimer laser was a promising technique for the corrosion protection of high-strength aluminum alloys in the aerospace applications. The rapid solidification of aluminum die cast alloys by the high-power laser radiation was examined by Haferkamp et al. (Ref 9). They correlated the heating and cooling rates with the resulting grain structures.

In the present study, laser melting of aluminum surface is considered and the heating model allowing the formation of mushy zones between the solid-liquid and the liquid-vapor phases is introduced. Temperature field and the resulting cavity shapes in the substrate material are predicted. Oxygen diffusion into the irradiated region during laser processing is examined and oxygen concentration around the region of the cavity surface is predicted. An experiment is carried out to resemble the conditions adopted in the simulations. The morphological and metallurgical changes in the irradiated region are examined using SEM, EDS, and XRD.

2. Mathematical Analysis

2.1 Heating Analysis

The Gaussian laser output power intensity distribution at the workpiece surface is assumed and its center is located at the center of the co-ordinate system. This results in an axisymmetric heating of the workpiece material. The temporal variation of laser power intensity resembling the actual laser pulse is used in the simulations. The heat conduction equation for a solid-phase heating due to a laser irradiation pulse with a Gaussian intensity profile can be written as:

$$\rho_s Cp_s \frac{\partial T}{\partial t} = \frac{k_s}{r}\frac{\partial}{\partial r}\left(r\frac{\partial T}{\partial r}\right) + k_s\frac{\partial^2 T}{\partial z^2} + S_o, \qquad \text{(Eq 1)}$$

where S_o is the volumetric source term and it is,

$$S_o = I_o\delta(1-r_f)\exp(-\delta z)\exp\left(-\frac{r^2}{a^2}\right), \qquad \text{(Eq 2)}$$

where I_o, δ, r_f, and a are the laser peak power intensity, absorption coefficient, reflectivity, and the Gaussian parameter, respectively.

The initial and boundary conditions for Eq 1 are given below. Initially, the substrate material is assumed at a uniform temperature, T_o, i.e.:

$$\text{At time zero} \Rightarrow t = 0 : T(r,z,0) = T_o \text{ (specified)}$$

At a distance considerably away from the surface (at infinity) in the radial direction a constant temperature T_o is assumed. Since the heating has no effect on the temperature rise at a depth of infinity below the surface, temperature is assumed to be constant and equals to the initial temperature of the substrate material in this region. The respective boundary conditions are:

$$r \text{ at infinity } \Rightarrow r = \infty : T(\infty,z,t) = T_o \text{ (specified)}$$
$$z \text{ at infinity } \Rightarrow z = \infty : T(r,\infty,t) = T_o \text{ (specified)}$$

At the symmetry axis, maximum temperature is assumed and the convection boundary condition is considered at the workpiece surface, i.e.:

$$\text{At symmetry axis } \Rightarrow r = 0 : \frac{\partial T(0,z,t)}{\partial r} = 0$$

and

$$\text{At the surface } \Rightarrow z = 0 : k\frac{\partial T(r,0,t)}{\partial z} = h(T(r,0,t) - T_o),$$

where h is taken as 10^3 W/m^{2}K due to natural convection from the surface (Ref 10).

Since the evaporation temperature depends on the pressure and this relation is not known for steel vapor, it is assumed that the substrate material has single melting and boiling temperatures. Moreover, once the phase change initiates, a mushy zone (mutually existence of two phases) is introduced across the interface of two phases. During the phase change process, including the mushy zone, temperature of the substrate material remains the same, but its enthalpy changes in this region. This situation can be formulated via energy balance in the mushy zone. It should be noted that nominal laser pulse length is 24 ns, therefore, the flow in the vapor and liquid layer during the heating process is neglected, i.e., 1 μm of fluid motion, in radial or axial direction, in the liquid layer requires the liquid velocity in the order of 1000 m/s, which may not be the case that occurs in the present simulations; consequently, during the short heating period, the fluid motion in the liquid and vapor phases is assumed not to influence the heat transfer mechanism in these zones.

The energy equation for the differential element in the mushy zone (Ref 11):

$$\rho_m L_m \frac{\partial x_m}{\partial t} = \frac{k_m}{r}\frac{\partial}{\partial r}\left(r\frac{\partial T}{\partial r}\right) + k_m \frac{\partial^2 T}{\partial z^2} + S_o \qquad \text{(Eq 3)}$$

Equation 3 is valid in the mushy zone (mutually existence of solid-liquid phases in the zone) where $0 \le x_m \le 1$, i.e., temperature of the cells with $0 \le x_m \le 1$ is set to melting temperature ($T = T_m$). x_m is the quality in the solid-liquid mushy zone, which is defined as $x_m = (m_l)/(m_l + m_s)$, where m_l and m_s are the mass of liquid and solid in the mushy zone. For the situation $x_m = 1$, liquid phase occurs and Eq 1 is used to determine the temperature rise in the liquid heating using the liquid thermal properties in the equation. Moreover, the liquid heating continues until the boiling point is reached in the substrate material; in which case, a new mushy zone is formed. In this case, Eq 3 is modified for a differential element in the mushy zone subjected to evaporation, i.e.:

$$\rho_b L_b \frac{\partial x_b}{\partial t} = \frac{k_b}{r}\frac{\partial}{\partial r}\left(r\frac{\partial T}{\partial r}\right) + k_b \frac{\partial^2 T}{\partial z^2} + S_o \qquad \text{(Eq 4)}$$

Equation 4 is applicable for temperature $T = T_b$ and $0 \le x_b \le 1$ in the mushy zone (partially liquid partially vapor zone); in which case, temperature of the cells with $0 \le x_b \le 1$ is set to the boiling temperature of the substrate material ($T = T_b$)·($T = T_m$). x_b is the quality in the liquid-vapor mushy zone, which is defined as $x_b = (m_v)/(m_v + m_l)$, where m_l and m_v are the mass of liquid and vapor in the mushy zone. It should be noted that x_m is replaced with x_b in Eq 4, which represents the fraction of vapor phase in the differential element. The calculation of x_b is the same as x_m, provided that latent heat of fusion is replaced with latent heat of evaporation of the substrate material in Eq 4 in the latter.

The boundary condition at the evaporating surface is introduced in relation to Eq 4. In this case, the temperature along the evaporated surface is kept at boiling temperature of the substrate material, i.e., the cells in the evaporated region are kept at boiling temperature, i.e.:

$$\text{In the mushy zone, at } z = z_b \Rightarrow T(r, z_b, t) = T_b,$$

where z_b represents the axial location at the evaporated surface.

Equations 3 and 4 provide the relative position of solid-liquid and liquid-vapor interface in the substrate material. Liquid-vapor interface determines the shape and size of the cavity generated during evaporation process.

2.2 Formulation of Oxygen Diffusion

Aluminum is resistant to oxidation and shows a very good affinity with oxygen. It is covered with a very thin layer of alumina (2–3 nm) at room temperature (Ref 12). Oxide formation can take place through oxygen adsorption on the metallic sites. The oxygen distribution in the metallic matrix depends on temperature, time, oxygen pressure, and crystallization state of the metal. Temperature-dependent diffusion coefficient of oxygen is used in the analysis. Since the Maragoni flow in the melt phase of the substrate material is neglected, the diffusion mechanism can be formulated from the second Fick's law. In this case, the governing diffusion equation in the axisymmetric coordinate system can be written as:

$$\frac{\partial C}{\partial t} = \frac{1}{r}\frac{\partial}{\partial r}\left(rD\frac{\partial C}{\partial r}\right) + \frac{\partial}{\partial z}\left(D\frac{\partial C}{\partial z}\right), \qquad \text{(Eq 5)}$$

where C is the nitrogen concentration and D is the diffusion coefficient. The relevant initial and boundary conditions are:

Initial condition:

At time zero: $t = 0 \rightarrow C(r, z, 0) = 0$

Boundary conditions:

z at infinity: $z = \infty \rightarrow C(r, \infty, t) = 0$

r at infinity: $r = \infty \rightarrow C(\infty, z, t) = 0$

At symmetry axis: $r = 0 \rightarrow ((\partial C(0, z, t))/(\partial r)) = 0$

At the surface: $z = 0 \rightarrow C(r, 0, t) = C_o$

where C_o is the oxygen concentration at the surface (0.16, based on the stoichiometry).

Equation 5 is solved numerically with the appropriate boundary conditions to obtained oxygen concentration in the substrate material.

3. Numerical Solution

Equation 1 is applicable to solid and liquid heating, Eq 3 is applicable to mushy zone at solid-liquid interface and Eq 4 is applicable to mushy zone at liquid-vapor interface. To discretize the governing equations, a finite difference scheme is introduced. The details of the numerical scheme are given in Ref 11 and 13. To compute the equations discretized for temperature field and relative positions of solid-liquid and liquid-vapor interface, an implicit scheme is used, i.e., using the initial conditions, the temperature in the whole domain is calculated for following time steps with the respective conditions. Moreover, implicit scheme is used for solving the oxygen diffusion equation (Eq 5), provided that temperature field-predicted previous simulations are used in the prediction of oxygen concentration.

The calculation domain is divided into grids and grid independence test is performed for different grid size and orientation and the grid size resulting from grid independent solution is used, which is 100×120 mesh points in the r and z-axes. A computer code based on implicit scheme is developed to predict the temperature field.

The material properties and pulse intensity used in the simulations are given in Tables 1 and 2, respectively, while Table 3 gives temperature-dependent oxygen diffusion coefficient (Ref 14). It should be noted that the laser pulse properties employed in the simulations resemble the actual pulse used in

Table 1 Thermal properties of aluminum used in the simulations

T_m, K	T_b, K	ρ, kg/m^3	Cp, J/kg/K	k, W/m/K	δ (1/m)	L_m, J/kg	L_b, J/kg
933	2720	2702	$-0.0003T^2 + 0.8713T + 631.75$	$-10^{-4}T^2 + 0.067T + 228$	6.17×10^6	3.21×10^5	1.1×10^6

Table 2 Laser pulse intensity used in the simulations

Peak intensity, W/m^2	Gaussian parameter, m	Nominal pulse length, ns
3.33×10^{12}	8.33×10^{-6}	24

Table 3 Temperature-dependent diffusion coefficient (Ref 14)

Temperature, K	D, m^2/s
293	1.3×10^{-20}
473	5.5×10^{-20}
673	5.1×10^{-20}
773	1.5×10^{-20}

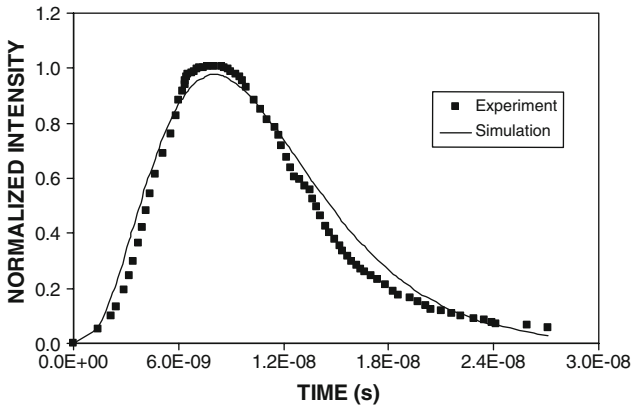

Fig. 1 Normalized laser pulse intensity used in the simulations

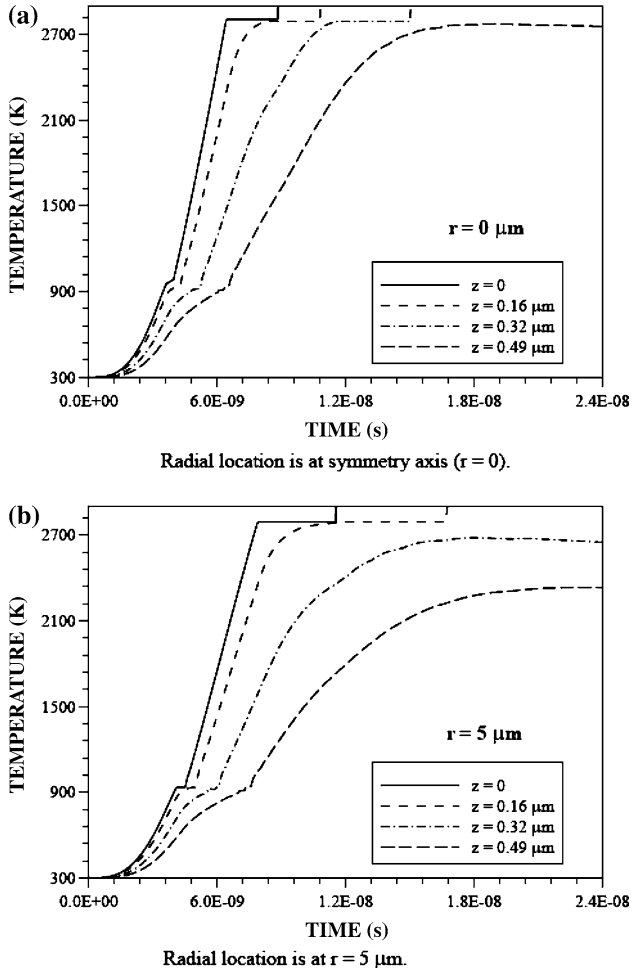

Fig. 2 Temporal variation of temperature at two radial locations and different depths

the experiment. The normalized pulse intensity is shown in Fig. 1.

4. Results and Discussions

Laser heating of aluminum surface is considered and the cavity formation at the surface is modeled. The mushy zones generated across the solid-liquid and the liquid-vapor phases are predicted and oxygen diffusion into the substrate material is determined during the laser heating process. An experiment resembling the simulation conditions is carried out to examine the morphological and metallurgical changes in the laser-irradiated region.

Figure 2 shows temporal variation of temperature along the symmetry axis (Fig. 2a) and at the radial location $r = 5$ μm (Fig. 2b) at different depths below the surface. In the solid phase, temperature rise is gradual in the early heating period and as the heating duration progresses it rises rapidly. This is more pronounced in the surface vicinity where $z \leq 0.16$ μm. This is because of the laser power absorbed in the surface region, which is higher than that of at some depth below the surface. It should be noted that the laser power absorbed by the substrate material decays exponentially with the depth below the surface (Lambert's law). Moreover, the gradual rise of temperature is because of the temporal distribution of the laser power intensity (Fig. 1), which is low in the early heating period. As the time progresses, the power intensity increases. This, in turn, results in the rapid rise of temperature within the absorption depth of the substrate material. Although convection heat transfer from the free surface and conduction from the surface vicinity to the solid bulk lower the internal energy gain from the irradiated field in the surface region; in which case, energy gain in the surface region becomes significantly high so that temperature rises continuously. This situation slightly differs at some depth below the surface due to the relatively low energy gain from the irradiated field in this region as compared to that of in the surface vicinity. Once the melting temperature of the substrate material is reached, the phase change takes place and temperature rise at the surface reduces significantly. It should be noted that during the initiation of the melting process, a mushy zone is formed; however, the duration of the mushy zone becomes small because of the high laser power intensity. This limits the duration of constant temperature during the melting process. As the time increases further, temperature rise becomes sharp in the regime of the super heating of liquid phase. This is more pronounced at the surface. However, at some depth below the surface, the rate of temperature rise is low because of the low irradiated energy absorbed in this region. Once the evaporation temperature of the substrate

material is reached, a mushy zone is formed across the liquid and vapor phases; in which case, temperature remains the same. Since the latent heat of evaporation is much higher than the latent heat of melting of the substrate material, the duration of constant temperature at evaporation temperature is longer than that of at the melting temperature. It should be noted that temperature rise beyond the evaporation temperature is not considered in the present study, since the plasma heating is avoided in the analysis. In the case of the radial location of r = 5 μm away from the symmetry axis, temperature profiles behave similar to those at the symmetry axis, provided that the rise of temperature in the solid and the liquid phases are not the same. This is because of the spatial distribution of the laser power intensity, which is Gaussian, i.e., power intensity reduces along the radial direction so that temperature rise reduces at the radial location away from the symmetry axis.

Figure 3 shows temperature distribution inside the substrate material for four heating periods and four radial locations. In the early heating period (t = 6 ns), temperature does not reach the evaporation temperature of the substrate material and mushy zone formation across the vapor and liquid phases is not possible. However, the mushy zone across the solid and liquid phases is evident. This situation is also seen from Fig. 4; in which the cross-sectional view of the phases formed in the substrate material at different heating durations is shown. The temperature gradient in the liquid region is larger along the symmetry axis than that of the other radial locations. This is because of the laser power intensity distribution in the radial direction, i.e., the laser power intensity reduces with the increasing radial distance from the symmetry axis. As the time progresses, temperature distribution in the mushy zone becomes visible, particularly across the liquid and vapor phases. However, the differences in temperature distributions corresponding to the different depths becomes more visible at t = 12 ns. This is because of the phase change process and the absorbed power intensity distribution in the radial direction. Energy absorbed from the irradiated field is mainly dissipated for the phase change process at the radial location$r$ = 15 μm away from the symmetry axis while super heating in liquid phase takes place in the region around the symmetry axis. As the time progresses further, the super heating in the liquid phase almost dominates the heating process, since the size of the liquid phase in the laser-irradiated region increases significantly. This is also evident from Fig. 4. Moreover, the size of the mushy zone across the solid and liquid phases is smaller than that corresponding to vapor mushy zone. This is because of the latent heat of evaporation, which is higher than the latent heat of fusion. Moreover, Fig. 5 shows the recession velocity predicted and obtained from the previous formulation (Ref 15). It can be observed that both results are in agreement. However, the differences in the values of the recession velocity are because of the one-dimensional consideration and the assumption of the constant properties in the previous formulation (Ref 15). Nevertheless, this difference is small.

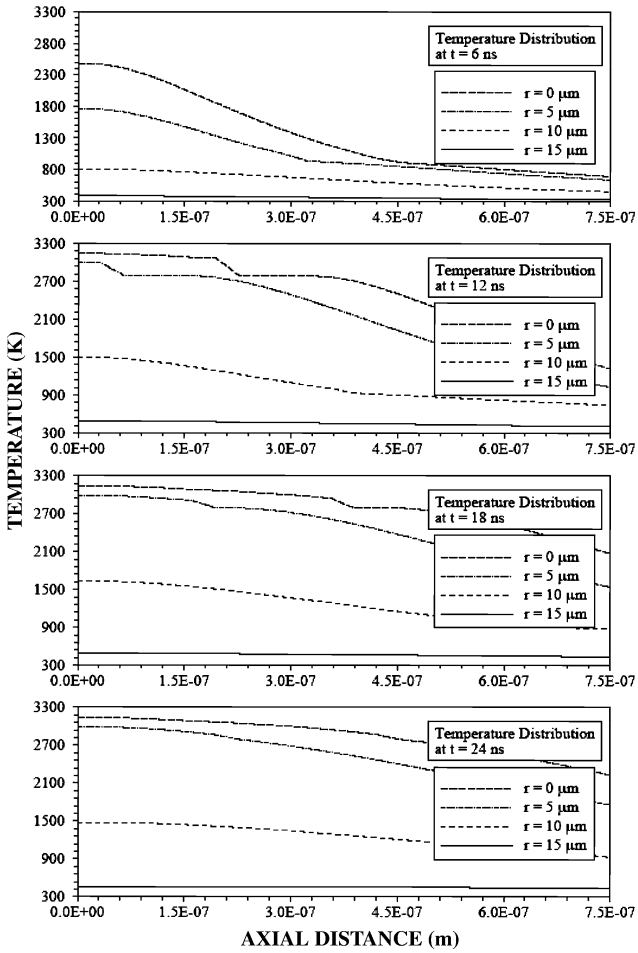

Fig. 3 Temperature distribution inside the substrate material at various radial locations and four heating durations

Figure 6 shows the contours of oxygen concentration in the laser-irradiated region. Since oxygen diffusion coefficient in aluminum is low, oxygen concentration remains high in the vicinity of the surface and as the depth below the surface increases, it decreases significantly. It should be noted that oxygen concentration is normalized through its maximum value which is based on the oxygen content (stoichiometric) in Al_2O_3 compound, i.e., the maximum oxygen concentration at the surface is 0.16 and the normalized value is 1. Moreover, oxygen concentration is high in the surface of the cavity and it reduces sharply with increasing depth below the surface. Since oxygen diffusion coefficient is temperature dependent and attains high values with increasing temperature, concentration remains high in the region of high temperature. Therefore, oxygen diffusion is high around the surface and its distribution follows the cavity shape. The sharp decay of oxygen concentration is also evident from Fig. 7, in which normalized oxygen concentration along the radial direction for two heating periods and at different depths below the surface is shown. The linear variation of the normalized concentration is because of the similar temperature range across the short distance in the radial direction. Moreover, the sharp decay of concentration indicates that oxygen diffusion is limited with a short distance in the radial direction.

Figure 8 shows SEM micrograph of the laser-irradiated surface and the cross-section of the irradiated region. The small-size cavity formation is evident at the surface and cracks are observed in and around the cavity. The surface is compact and the depth of the cavity is very shallow as similar to the maximum depth predicted after the laser pulse ending (1.5 μm). The melt layer and the heat-affected zone are not clearly identifiable due to the microstructure

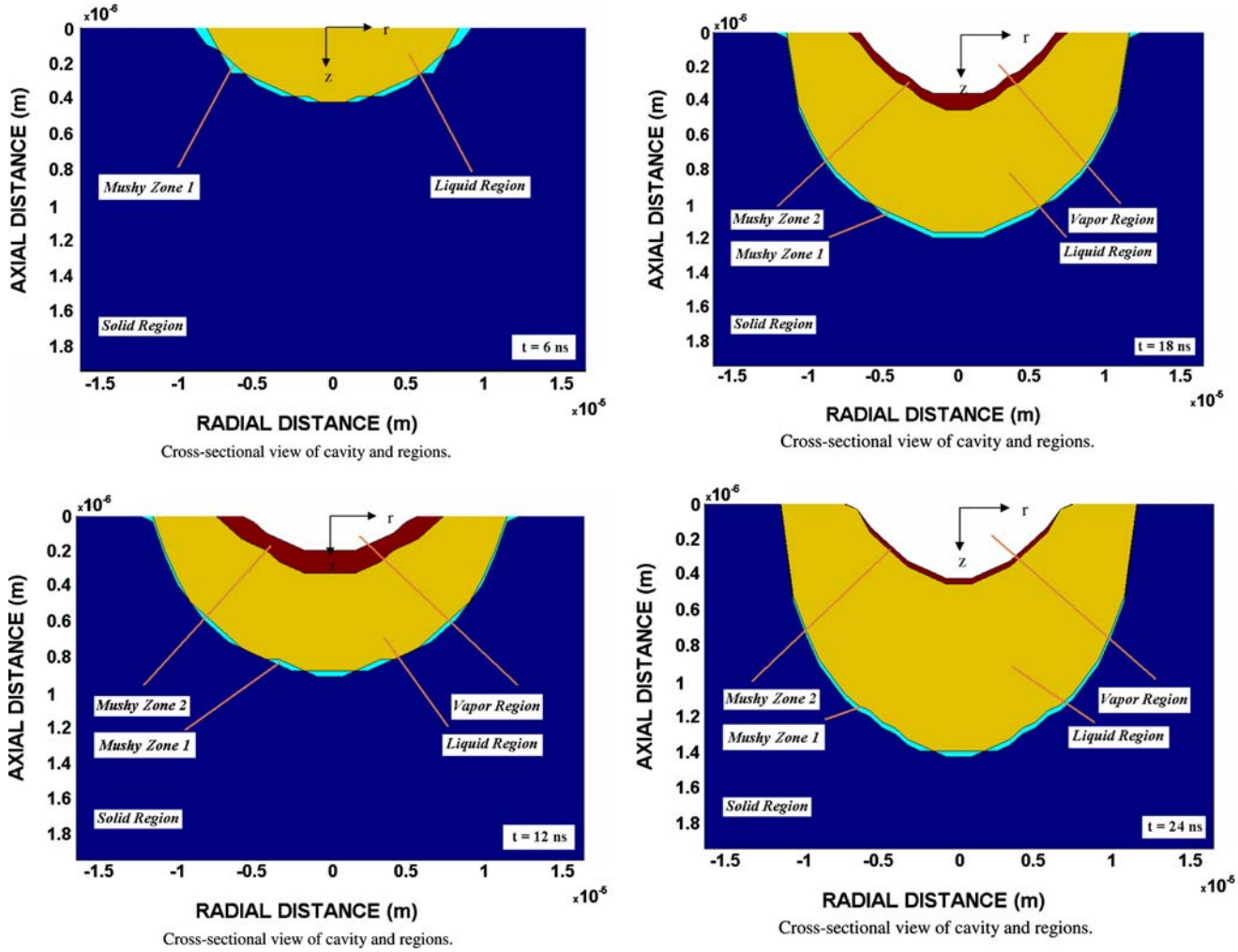

Fig. 4 Cavity cross sections and regions for different heating periods. Mushy zone 1 corresponds to the solid-liquid phases while mushy zone 2 is the liquid-vapor phases

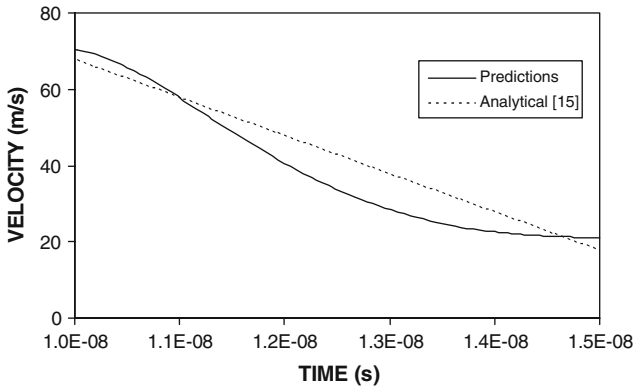

Fig. 5 Recession velocity predicted and obtained from previous study (Ref 15)

developed below the cavity. The delamination and voids in the irradiated region are not evident from the cross-sectional view. The shallow cavity is also evident from micrograph obtained from the atomic force microscopy (Fig. 8). Consequently, the depth of the cavity formed in the surface region of the substrate material is shallow due to the single laser pulse irradiation.

5. Conclusions

Laser evaporative heating of aluminum surface is considered and the mushy zones formation across the solid and liquid and the liquid and the vapor phases are modeled. Temperature rise inside the substrate material and the cavity shape are predicted numerically. Temperature-dependent properties are used in the simulations. The experiment resembling the simulation conditions is carried out and the morphological changes in the irradiated zone are examined using SEM. It is found that temperature rise in the early heating period is gradual due to the temporal variation of the laser power intensity; however, temperature rise in the liquid phase is rapid. This is more pronounced along the symmetry axis, since the laser power intensity distribution at the irradiated surface is Gaussian. As the depth below surface increases, the rate of temperature rise

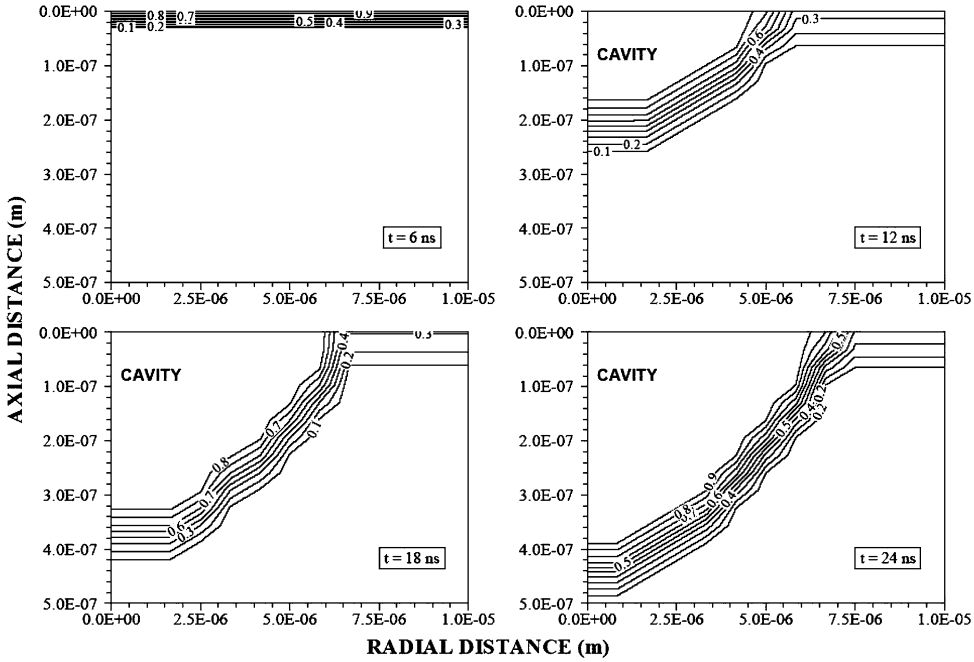

Fig. 6 Contours of normalized oxygen concentration obtained for four heating periods

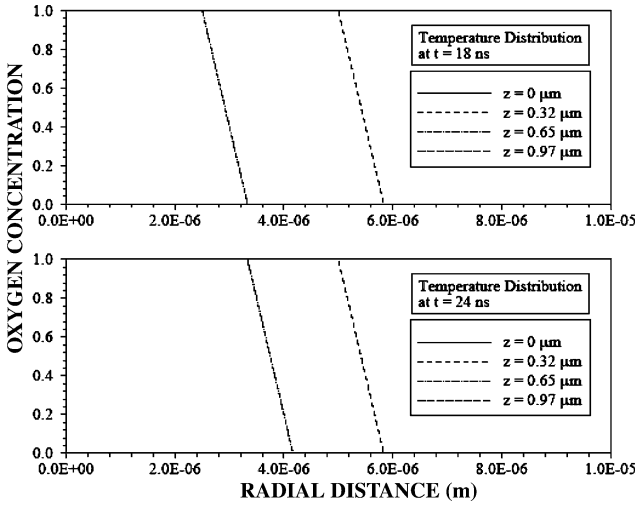

Fig. 7 Normalized oxygen concentration along the radial distance at different depths and for two heating periods

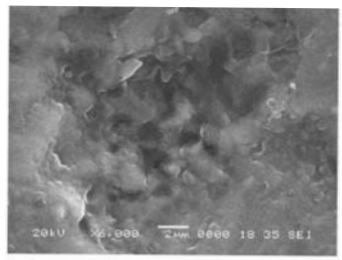

SEM micrograph of the top view of the laser produced cavity

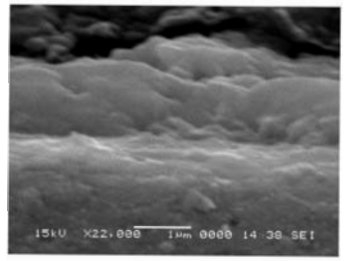

SEM micrograph of the cross-sectional view of the laser produced cavity

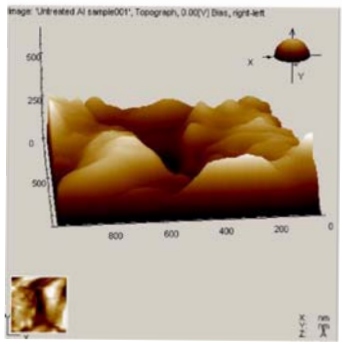

AFM micrograph of laser produced cavity

Fig. 8 SEM and ATM micrographs of laser-produced cavity

reduces because of less absorbed laser power in this region. The size of the mushy zone across the solid and the liquid phases is smaller than that of across the liquid and the vapor mushy zone. This is because of the latent heat of evaporation, which is higher than the latent heat of fusion. The depth of the liquid zone increases significantly with the progressing heating duration. This is attributed to the low melting temperature of the substrate material. Oxygen concentration reduces sharply with increasing depth below the surface due to low oxygen diffusion coefficient. The cavity formed in the surface region is shallow, which can be observed from the SEM and AFM

micrographs. This agrees with the numerically predicted cavity depth at the end of the heating pulse.

Acknowledgment

The authors acknowledge the support of King Fahd University of Petroleum and Minerals, Dhahran, Saudi Arabia for this work.

References

1. A. Koutsomichalis and A. Kefalidou, Excimer Laser Interactions with an Aluminum Alloy, *J. Laser Appl.*, 1996, **8**(5), p 247–250
2. T.M. Yue, C.F. Dong, L.J. Yang, and H.C. Man, The Effect of Laser Treatment on Stress Corrosion Cracking Behavior of 7075 Aluminum Alloy, *Mater. Lett.*, 2004, **58**, p 630–635
3. K.G. Watkins, Z. Liu, M. McMahon, R. Vilar, and M.G.S. Ferreira, Influence of the Overlapped Area on the Corrosion Behaviour of Laser Treated Aluminum Alloys, *Mater. Sci. Eng. A*, 1998, **252**(2), p 292–300
4. G. Gomez-Rosas, C. Rubio-Gonzalez, J.L. Ocaña, C. Molpeceres, J.A. Porro, W. Chi-Moreno, and M. Morales, High Level Compressive Residual Stresses Produced in Aluminum Alloys by Laser Shock Processing, *Appl. Surf. Sci.*, 2005, **252**(4), p 883–887
5. T. Kikuchi, S.Z. Chu, S. Jonishi, M. Sakairi, and H. Takahashi, Laser Surface Modification of Aluminum by Laser Irradiation, *Electrochim. Acta*, 2001, **47**, p 225–234
6. V.I. Mazhukin, V.V. Nossov, and I. Smurov, Analysis of Laser-Induced Evaporation of Al Target Under Conditions of Vapour Plasma Formation, *Thin Solid Films*, 2004, **453–454**, p 353–361
7. S. Valette, R. Le Harzic, E. Audouard, N. Huot, R. Fillit, and R. Fortunier, X-ray Analysis of Mechanical and Thermal Effects Induced by Femtosecond Laser Treatment of Aluminum Single Crystals, *Appl. Surf. Sci.*, 2006, **252**(13), p 4691–4695
8. A.J. Davenport, N. Tareelap, C. Padovani, B.J. Connolly, S.W. Williams, E. Siggs, D.A. Price, Corrosion Protection of Aerospace Aluminum Alloys With Laser Surface Melting, *Meeting Abstracts, 208th Meeting of The Electrochemical Society*, v MA 2005-02, 2005, p 551
9. H. Haferkamp, F. Von Alvensleben, and O. Thurk, Rapid Solidification of Aluminum Diecast Alloys by High Power Laser Radiation, *Proc. SPIE*, 1998, **3414**, p 44–50
10. S.Z. Shuja, B.S. Yilbas, and M.O. Budair, Modeling of Laser Heating of Solid Substance Including Assisting Gas Impingement, *Numer. Heat Transfer, Part A*, 1998, **33**, p 315–339
11. I.Z. Naqavi, "Conduction and Non-Conduction Limited Laser Heating Process – Mathematical Simulation," M.Sc. Thesis, Mech. Eng. Dept., KFUPM, 2001
12. K. Shimizu, R.C. Furneaux, G.E. Thompson, G.C. Wood, A. Gotoh, and K. Kobayashi, On the Nature of 'Easy Paths' for the Diffusion of Oxygen in Thermal Oxide Films on Aluminum, *Oxid. Metals*, 1991, **35**(5–6), p 427–439
13. S.V. Patankar, *Numerical Heat Transfer.* McGraw-Hill, New York, 1980
14. M. Garcia-Mendez, N. Valles-Villarreal, G.A. Hirata-Flores, and M.H. Farias, Study of Thermal Diffusion Between Al_2O_3 and Al Thin Films, *Appl. Surf. Sci.*, 1999, **151**(1), p 139–147
15. M. Kalyon and B.S. Yilbas, Analytical Solution for Laser Evaporative Heating Process: Time Exponentially Decaying Pulse Case, *J. Phys. D: Appl. Phys.*, 2001, **34**, p 3303–3311